Cancer Therapy: Preclinical

Clinical Cancer Research

Radioimmunotherapy of Fibroblast Activation Protein Positive Tumors by Rapidly Internalizing Antibodies

Eliane Fischer[1,2], Krishna Chaitanya[1], Thomas Wüest[1], Andreas Wadle[1], Andrew M. Scott[3], Maries van den Broek[1], Roger Schibli[2], Stefan Bauer[1], and Christoph Renner[1]

Abstract

Purpose: Fibroblast activation protein (FAP) is a serine protease that has emerged as a promising target for cancer therapy, either by direct abrogation of its proinvasive activity or by specific targeting of FAP-expressing cells with cytotoxic immunoconjugates. We aimed to select novel human–mouse cross-reactive antibodies and to test suitability for tumor therapy as radioimmunoconjugates in a preclinical model.

Experimental Design: Human Fab fragments that bind to human and murine FAP were selected from an antibody phage library. Two candidates (ESC11 and ESC14) were engineered into fully human IgG1 antibodies and further characterized. We investigated the intracellular trafficking of ESC11 and ESC14 in live cells by confocal microscopy and analyzed the biodistribution and therapeutic effects of anti-FAP antibodies labeled with the β-emitting radionuclide ^{177}Lu in a melanoma xenograft nude mouse model. Results were compared with vF19, a humanized variant of an anti-FAP antibody that has been previously used in clinical trials.

Results: The two antibodies bound selectively to both human and mouse FAP, with affinities in the low nanomolar range. Binding to FAP-expressing melanoma cells resulted in rapid internalization of FAP-antibody complexes. ^{177}Lu-labeled ESC11 specifically accumulated in melanoma xenografts *in vivo*, with a higher tumor uptake than ESC14 and vF19. Radioimmunotherapy with 8 MBq ^{177}Lu-labeled anti-FAP antibodies delayed growth of established tumors, whereas ^{177}Lu-ESC11 extended mouse survival more pronounced than ^{177}Lu-ESC14 and ^{177}Lu-vF19.

Conclusion: Our results show the potential of ESC11 and ESC14 as potent radioimmunoconjugates or antibody–drug conjugates for diagnostic and therapeutic use in patients with FAP-expressing tumors. *Clin Cancer Res; 18(22); 6208–18. ©2012 AACR.*

Introduction

Fibroblast activation protein (FAP) has emerged as a key player in cancer physiology with multiple biologic functions. Most prominently, FAP is highly expressed on carcinoma-associated fibroblasts where it is thought to contribute to cancer initiation, progression, and metastasis (1–3). In addition, FAP is also present in some cancer cells, including bone and soft tissue sarcoma (4) and some melanoma (5) cells. FAP is a type II transmembrane serine protease that gains its enzymatic activity upon homodimerization of 2 identical 97 kDa subunits (6, 7). The natural substrates of FAP are still not completely identified, but the protease is capable of cleaving N-terminal dipeptides from polypeptides with proline or alanine in the penultimate position (8) and also has collagenase activity (9–11). The dipeptidyl-peptidase activity of FAP is one of the mediators of tumor progression (12), extracellular matrix remodeling (13–18), and metastasis formation (10, 19), but recent studies strongly suggest additional effects of FAP in the absence of its enzymatic activity (20) by hitherto unclear mechanisms. Very recently, FAP-expressing stromal cells have been shown to suppress antitumor immunity (21), adding yet another aspect to the manifold contributions of FAP to tumor growth.

Because of this multifaceted influence on tumor physiology, its restricted expression pattern within diseased areas and correlation with poor clinical outcome in patients with cancer (22, 23), FAP has emerged as a promising target for cancer therapy. A humanized version of mAb F19 (sibrotuzumab), a first generation anti-FAP antibody, however,

Authors' Affiliations: [1]Division of Oncology, University Hospital Zürich, Zürich; [2]Center for Radiopharmaceutical Sciences, Paul Scherrer Institute, Villigen, Switzerland; and [3]Ludwig Institute for Cancer Research, Melbourne, Australia

Note: Supplementary data for this article are available at Clinical Cancer Research Online (http://clincancerres.aacrjournals.org/).

E. Fischer and K. Chaitanya contributed equally to this article.

Corresponding Author: Christoph Renner, Oncology Department, Universitätsspital Zürich, 8091 Zürich, Zurich, Switzerland. Phone: 41-44-255-8902; Fax: 41-44-255-4548; E-mail: christoph.renner@usz.ch

doi: 10.1158/1078-0432.CCR-12-0644

©2012 American Association for Cancer Research.

Downloaded from http://aacrjournals.org/clincancerres/article-pdf/18/22/6208/2007966/6208.pdf by guest on 17 February 2026

Johns Hopkins University EX2031
GE Healthcare v. Johns Hopkins
IPR2026-00069

Translational Relevance

Carcinoma-associated fibroblasts in epithelial cancers and tumor cells of melanoma or sarcoma origin express high levels of fibroblast activation protein (FAP). In phase I/II clinical trials, first generation FAP-specific antibodies have shown high tumor-selective expression of this antigen. The novel antibodies described in this study, ESC11 and ESC14, rapidly internalize into FAP-expressing cells and exhibit excellent *in vivo* targeting properties. Therefore, they are ideal scaffolds for the development of immunoconjugates with cytotoxic drugs or radiometals that are retained within the cells. Our preclinical studies using a melanoma model serve as a basis for the clinical development of the ESC11 and ESC14 antibodies for targeting FAP-expressing tumor cells or carcinoma-associated fibroblasts. As both antibodies cross-react with rodent FAP, the relevance of preclinical studies is increased. Furthermore, translation to the clinic is facilitated because they are fully human antibodies.

failed to show measurable therapeutic activity (24) in phase I/II clinical trials despite excellent tumor stroma targeting properties (25). In addition, 8 of 26 sibrotuzumab-treated patients developed human–anti-human antibodies (HAHA) with a change in pharmacokinetics and reduced tumor uptake in 4 of them. Therefore, further clinical development of sibrotuzumab was halted.

Strategies to target cancer with modified FAP-specific antibodies have recently gained interest and new technologies for the conjugation of toxins or cytokines to FAP-specific antibodies have been established. For example, an antibody–maytansinoid conjugate (26) and antibody–TNF fusion proteins (27, 28) have shown promise at the preclinical stage and are pending clinical development.

Radioimmunotherapy, the targeted delivery of therapeutic radioisotopes to the tumor site by monoclonal antibodies, is an attractive strategy for cancer treatment. Notably, antigen expression is usually spatially heterogeneous within the tumor. With FAP being restricted to carcinoma-associated fibroblasts, the therapeutic efficacy can be augmented by the "cross-fire" effect of β-emitting radionuclides on neighboring FAP-negative tumor cells. Clinical trials with ^{131}I-labeled sibrotuzumab have been conducted to investigate targeting properties and pharmacokinetics but were discontinued because of the above-mentioned issues associated with HAHA (25). While radioiodination with ^{131}I is relatively easy to conduct, the radionuclide is readily released from the tumor upon internalization into cells. In contrast, high doses of residualizing radioisotopes may accumulate at the tumor site with internalizing antibodies and lead to a persistent irradiation of the tumor tissue. The radiolanthanide ^{177}Lu has a comparable range of the β-particles in tissue as ^{131}I (2 and 3 mm, respectively). In contrast to the high energy γ-photons of ^{131}I, which are a disadvantage from a radiation safety perspective, ^{177}Lu emits 208 keV γ-photons at much lower abundance (11%).

For preclinical evaluation of radioimmunoconjugates, human–mouse cross-reactive antibodies are preferentially used to detect possible accumulation in tissue expressing homologous FAP. This allows more accurate estimation of side effects that may arise from radioactive doses delivered to healthy organs. In addition, for targeting of the tumor stroma in preclinical models, crossreactivity with the homologous antigen of the model species is a prerequisite.

In this report, we describe the successful selection of 2 human monoclonal antibodies, ESC11 and ESC14, from a phage-display library. In contrast with F19 (sibrotuzumab), we found that these novel antibodies were rapidly internalized by FAP-positive cells. Using ESC11 and ESC14 labeled with the β-emitting radiolanthanide ^{177}Lu, we found that both antibodies specifically accumulated in xenografted FAP-positive human melanoma and delayed tumor growth *in vivo*.

Materials and Methods

Cells, cell lines, and reagents

HEK293huFAP, HEK293muFAP, and HEK293huCD26 were generated by cloning huFAP, CD26, or muFAP cDNA into the pEAK8 vector (Edge Biosystems) and stable transfection of HEK293 c-18 cells (ATCC CRL-10852) followed by monoclonalization by limited dilution. The cell lines were maintained in Dulbecco's modified Eagle's medium supplemented with 10% FBS, penicillin–streptomycin, and puromycin (3 μg/mL). HT1080 FAP$^+$, huFAP-expressing HT1080 [American Type Culture Collection (ATCC) CCL-121], were maintained in RPMI supplemented with 10% FBS (Gibco, Invitrogen) and 200 μg/mL G418. Human melanoma cell lines SK-Mel-187 and SK-Mel-16 were kindly provided by Ludwig Institute for Cancer Research (New York) and maintained in RPMI 10% FBS. Murine antibody F19 and human anti-A33 antibody were obtained from Ludwig Institute for Cancer Research (Melbourne, Australia). Humanized vF19 was generated by veneering of F19 and was supplied by the Ludwig Institute for Cancer Research.

Antibody selection by phage display

For selection of huFAP-muFAP–specific antibodies, a nonimmunized phage library–expressing human antibody Fab fragments was used (29). Details of the selection procedure are outlined in the Supplementary Data.

Phage screening by ELISA

For screening of FAP-binding phage by ELISA, 96-well microtiter plates (MaxiSorp Nunc) were coated with cell extracts from HEK293 huFAP, HEK293 huCD26, HEK293 muFAP, or mock-transfected HEK293, blocked with 5% milk powder in PBS, incubated with phage-containing supernatants for 1 hour at room temperature, and developed using an anti-M13-HRP–conjugated antibody and tetramethylbenzidin as substrate.

Downloaded from http://aacrjournals.org/clincancerres/article-pdf/18/22/6208/2007966/6208.pdf by guest on 17 February 2026

Expression of fab fragments

Fab fragments were produced in *E. coli* TG-1 by induction with 1 mmol/L isopropyl-l-thio-B-[scap)d[r]-galactopyranoside (IPTG) for 4 hours at 30°C. Soluble Fab was released from the periplasmic fraction by incubation in PBS, pH 8 at 4°C overnight. Crude fractions were incubated with Talon resin (CLONTECH Laboratories) for 1 hour at 4°C, washed with wash buffer (20 mmol/L Tris, 100 mmol/L NaCl, 0.1% Tween 20), eluted with 100 mmol/L imidazole, and dialyzed against PBS at 4°C overnight.

Determination of kinetic rate constants and affinity by surface Plasmon resonance

Binding analysis of Fabs was conducted on a BIAcore T100 instrument. Recombinant huFAP (R&D systems) was immobilized at low density on a CM5 sensor chip (Biacore AB) using amine coupling chemistry according to the manufacturer's instructions. ESC11 and ESC14 Fabs were injected in 10 mmol/L HEPES, pH 7.4, 3.4 mmol/L EDTA, 0.15 mmol/L NaCl, and 0.005% Tween 20 at a flow rate of 80 μL/min at 25 °C, and concentrations ranging from 0.5 to 16 nmol/L and 6.25 to 200 nmol/L, respectively. The sensor chip was regenerated between injections with 0.1 mol/L sodium carbonate and rate constants were calculated using BIAevaluation data analysis program.

Cloning, expression, and purification of IgG1

The variable sequences of heavy and light chain were cloned via DraIII and RsrII sites, respectively, into a modified pEE12.4 vector (LONZA Biologics) encoding human constant IgG1 domains. Stable antibody-producing cell lines were developed using NS0 cells and the glutamine synthetase selection system according to the manufacturer's instruction (LONZA Biologics). Human IgG were purified from the culture supernatant by binding to CaptureSelect Fab kappa Affinity Matrix (CaptureSelect) followed by elution with 0.1 mmol/L glycine pH 2.5 and dialysis against PBS at 4°C overnight.

Flow cytometry

Cells were harvested at 50% confluence and stained with primary and secondary antibodies for 60 and 30 minutes on ice, respectively. Each staining step was followed by 2 washing steps (1 mL PBS and 2% FBS). Cells were fixed with 2% paraformaldehyde for 10 minutes on ice before conducting flow cytometry. At least 10,000 cells were measured on a FACScan (BD) cytometer and analyzed using FlowJo software (Treestar). For determination of the apparent K_D, the mean fluorescence intensities of a serial dilution were plotted and a dose–response curve was fitted using the equation $f = Bmax^{*}abs(x)/(K_Dapp+abs(x))+Ns^{*}x$ with SigmaPlot software (Systat Software Inc.). Human primary antibodies were detected with FITC/DyLight488 conjugated goat-anti-human antibody, (Jackson Immunoresearch, cat. no. 109-485-003; 1:200 dilution), whereas murine antibodies were stained with anti-mouse DyLight 488-labeled antibody (Jackson Immunoresearch, cat. no.115-486-146; 1:200 dilution). Fab antibodies were detected with anti-myc tag antibody 9E10, followed by an anti-mouse immunoglobulin-PE conjugate, (Jackson Immunoresearch, cat. no. 115-165-003; 1:200 dilution). Quantification of cell-surface FAP in internalization experiments was conducted after overnight incubation with human IgGs at 37°C. Cells were then stained with 10 μg/mL F19 followed by anti-mouse FITC-conjugated antibody and % FAP expression was calculated relative to the mean fluorescence intensity of cells that have not been incubated with human IgG. In case of vF19, directly labeled ESC11 (DyLight 549) was used to detect cell-surface FAP.

Confocal microscopy

Cells were seeded on sterile 20 mm fibronectin-coated (Sigma F1141-1MG, at 10 μg/mL) coverslips (Deckglaser; Carolina Biological) in 12-well plates and grown to 20 to 30% confluency. Cells were fixed with 2% paraformaldehyde on ice and permeabilized using Cytofix/Cytoperm solution (51-2090KZ; BD Biosciences). Primary antibodies were diluted in 1× Perm/Wash (51-2091KZ; BD Biosciences) at following dilutions: EEA1, 1:100 (2411; Cell Signaling Technologies), LAMP1, 1:1,000 (ab24170; Abcam), F19, 1:100. All secondary antibodies were used at a 1:200 dilution and were obtained from Jackson Immunoresearch. Dynasore hydrate (D7693; Sigma) and 5-(N-ethyl-N-iso-propyl) amiloride (EIPA; A3085; Sigma) were added 30 minutes before the experiment at a final concentration ranging from 0 to 100 μmol/L and 0 to 10 μmol/L, respectively. Cells were fixed with 4′, 6-diamidino-2-phenylindole antifade (Invitrogen). All images were acquired on Leica SP5 UV/Vis confocal microscope (Leica Microsystems) at the Center for Microscopy and Image Analysis (University of Zurich, Zurich, Switzerland) using LAS AF software. Images were kept in 1024 × 1024 formats and acquired with a zoom factor of 4 at 700 Hz frequency with HCxAPO Lambda blue 63.0× oil UV objective lens at a numerical aperture of 1.40. Images were stored in Tagged Image File Format (TIFF) and further processed using Image J software.

For internalization experiments, cells were incubated with 30 μg/mL human IgGs for the indicated time. FAP was then detected with F19 and DyLight 549 anti-mouse antibody, (Jackson Immunoresearch, cat. no. 115-506-062; 1:200 dilution). After incubation with vF19, FAP was detected with directly conjugated ESC11-DyLight 549. Alternatively, internalization was directly induced and monitored by DyLight 549-conjugated human IgG1 (30 μg/mL).

Radiolabeling and quality control

Antibodies were labeled with ^{177}Lu using the chelator CHX-A″-DTPA (*N*-[(R)-2-Amino-3-(*p*-isothiocyanato-phenyl) propyl]-*trans*-(*S*,*S*)- cyclohexane-1,2-diamine-*N*,*N*′,*N*″,*N*″-pentaacetic acid, B355; Macrocyclics). Conjugation was conducted in borate buffer (0.07 mol/L, pH 9.15) under metal-free conditions and using a 5-fold molar excess of CHX-A″-DTPA. The reaction mixture was incubated for 1 hour at 37°C. For all antibodies, 0.5 to 1 moles CHX-A″-DTPA, were coupled per one mole IgG1, as determined by incubation of a fixed amount of conjugated antibody with

Downloaded from http://aacrjournals.org/clincancerres/article-pdf/18/22/6208/2007966/6208.pdf by guest on 17 February 2026

increasing amounts of ^{111}In (Mallinckrodt). The conjugated antibody was separated from free CHX-A″-DTPA using a NAP-5 column equilibrated with ammonium acetate buffer (0.25 mol/L, pH 5.5). CHX-A″-DTPA-antibody conjugates were labeled with ^{177}Lu ([^{177}Lu]Cl_3 in 0.04 mol/L HCl, ITG Isotope Technologies Garching-GmbH) for 1 hour at 37°C.

The reaction was quenched with 5 mmol/L EDTA and after 5 minutes of incubation at 37°C, the radiolabeled antibody was purified on a Superose-12 FPLC column (Amersham Biosciences). Elution was carried out in PBS at a flow rate of 0.5 mL/min. Radiochemical purity was analyzed by fast protein liquid chromatography (FPLC). The immunoreactive fraction was determined on HT1080 FAP cells using the Lindmo method as previously described (30).

SPECT/CT

Post mortem SPECT scans (2 hours 180 seconds/view) were conducted with a 4-head multiplexing multipinhole camera (NanoSPECT/CT; Bioscan Inc.) 72 hours after injection of ^{177}Lu-CHX-A″-DTPA-IgG1 (8 MBq, 15 μg) into the tail vein of nude mice bearing an SK-MEL-187 tumor on the hind leg and an SK-MEL-16 tumor on the shoulder. SPECT data were reconstructed iteratively with HiSPECT software (Scivis GmBH). The fused SPECT and CT datasets were analyzed using InVivoScope post processing software (Bioscan Inc.).

Biodistribution of ^{177}Lu-labeled antibodies in nude mice bearing human FAP-positive SK-Mel-187 tumors

Female nu/nu mice (Charles River) were injected subcutaneously in the right hind leg with 5×10^6 SK-Mel-187 cells in RPMI: BD Matrigel (cat. 354248; BD Biosciences) = 1:1 in a final volume of 200 μL. Tumors were allowed to grow to approximately 200 mm^3 before animals were randomly divided into groups of 6 mice for biodistribution studies (4 mice for time-dependent biodistribution of ^{177}Lu-ESC11). Four micrograms (3 MBq) of each radiolabeled antibody was injected intravenously in 100 μL PBS. Animals were sacrificed by cervical dislocation. Radioactivity for each organ was measured using a gamma counter. The experiments were approved by the local ethics committee for animal research.

Radioimmunotherapy with ^{177}Lu-labeled antibodies in nude mice bearing SK-Mel-187 tumors

Mice were injected subcutaneously with 5×10^6 FAP-positive SK-Mel-187 cells as described above and randomized into groups of 7 to 8 mice. 8 MBq radiolabeled antibody (100 μL in PBS, 15–17 μg) or 100 μL PBS was injected into the tail vein 5 days after tumor cell implantation. Tumor growth was measured every 2 to 3 days with a caliper and tumor volumes were calculated according to the formula: volume = length × width^2 × 0.52. Animals were sacrificed when tumor volumes exceeded 1,000 mm^3. Additional mice were sacrificed 3 and 7 days after treatment with 8 MBq ^{177}Lu-ESC11 or ^{177}Lu-A33 and tumors were processed for immunohistochemistry.

Immunohistochemistry experiments

Whole sections (3 μm thickness) were cut from formalin-fixed, paraffin-embedded blocks. Tissues were mounted on glass slides and deparaffinized in xylene. Rehydration was carried out in decreasing concentrations of ethanol and stained with hematoxylin–eosin using standard histologic techniques. Ki-67 immunohistochemistry was conducted using the automated Bond Max platform (Leica Microsystems) with a rabbit monoclonal MIB-1 antibody (1:200; clone SP6, Neomarkers, LabVision). Heat-induced epitope retrieval pretreatment was conducted using H2-Buffer (Leica Microsystems) and boiling at 95°C for 30 minutes. Bound antibody was detected with a corresponding secondary antibody included in the Refine-DAB detection kit (Leica Microsystems).

Statistical analyses

Data were analyzed using Prism (version 5.01) software (Graph Pad). Survival times were analyzed by Kaplan–Meier analysis, followed by the log-rank test. To correct for multiple comparisons of survival times, the Bonferroni-corrected threshold was applied to determine significance.

Results

Selection and characterization of mouse–human FAP cross-reactive antibody Fab fragments

Monoclonal antibody Fab-fragments were selected from a large human Fab antibody library by phage display. The first 4 panning rounds were conducted on human FAP (huFAP; Supplementary Fig. S1). Enrichment for Fab-fragments that crossreacted with mouse FAP (muFAP) was conducted in the fifth panning round (Supplementary Table S1). Screening of 300 selected clones by ELISA followed by PCR fingerprinting and sequencing of FAP-specific binders (data not shown) led to the identification of Fabs ESC11 and ESC14. By ELISA, both Fab fragments specifically bound to huFAP and muFAP and did not crossreact with the homologous protein CD26 (Fig. 1A). Furthermore, Fab ESC11 and ESC14 bound to native FAP on the cell membrane of muFAP or huFAP-expressing cells (Fig. 1B). The binding affinity to recombinant huFAP was determined by surface plasmon resonance measurement using chips coated with a low density of huFAP. K_D values of 10 ± 5 nmol/L and 210 ± 35 nmol/L were calculated for Fabs ESC11 and ESC14, respectively (Fig. 1C). Similar affinities were determined by flow cytometry with calculated $K_D$apps on huFAP-expressing cells of 4.7 ± 1.6 nmol/L for ESC11 and 200 nmol/L for ESC14, respectively (Table 1). On muFAP-expressing cells, $K_D$apps were 51 ± 11 nmol/L for ESC11 and 251 ± 42 nmol/L for ESC14 (Table 1).

Preparation and characterization of IgG1 antibodies ESC11 and ESC14

The variable heavy chain and light chain domains of ESC11 and ESC14 were cloned and expressed as fully human IgG1. IgG1 was purified by affinity chromatography from cell culture supernatant to more than 95% purity (Supplementary Fig. S2). As expected, the binding affinity

Downloaded from http://aacrjournals.org/clincancerres/article-pdf/18/22/6208/2007966/6208.pdf by guest on 17 February 2026

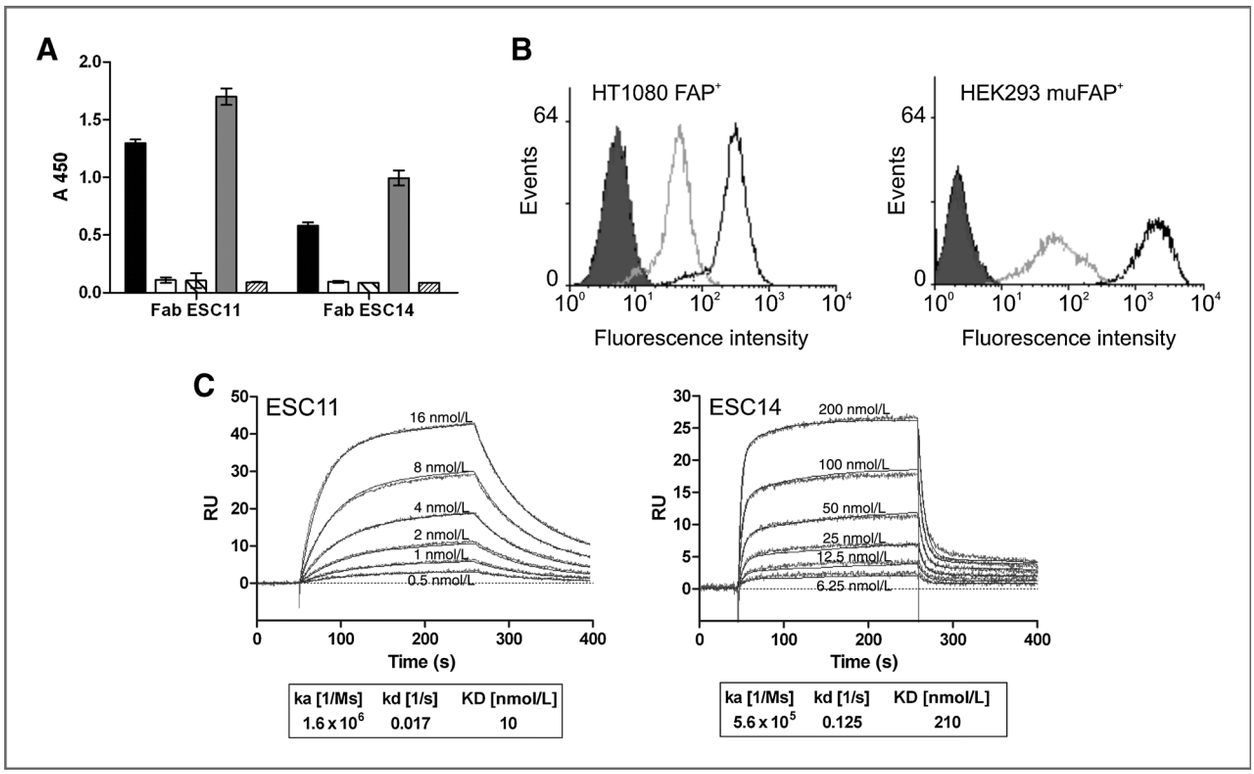


Figure 1. Specificity and affinity of Fabs ESC11 and ESC14. A, binding of Fabs ESC11 and ESC14 (100 nmol/L) in ELISA to plate immobilized membrane fractions of HT1080 FAP$^+$ (black bars), HT1080 (white bars), HEK293 huCD26$^+$ (striped bars), HEK293 muFAP$^+$ (grey bars), HEK293 mock–transfected line (hatched bars). B, fluorescence-activated cell sorting (FACS) analysis of Fab ESC11 (black line), ESC14 (grey line), and a nonbinding control Fab (filled) on HT1080 FAP$^+$ cells (left) and 293 muFAP$^+$ cells (right). C, affinity of Fabs ESC11 (left) and ESC14 (right) was determined by surface plasmon resonance. Purified Fabs were injected at the indicated concentrations on a rhuFAP-coated CM5 sensor chip.

of bivalent IgG1 for huFAP was higher than that of monovalent Fab due to avidity effects with apparent K_D values around 1.1 nmol/L on huFAP for both ESC11 and ESC14 IgGs (Table 1). These binding affinities are about 4-fold higher than for vF19 IgG. Interestingly, affinity constants of both ESC11 and ESC14 for muFAP were similar (around 2 nmol/L) after conversion to IgG1.

Epitope mapping by competitive binding assay

To investigate whether ESC11 and ESC14 recognize different epitopes of FAP, we used ESC11 to compete with ESC14 or F19 for binding to native surface human FAP and vice versa followed by flow cytometry. Binding of ESC11 Fab could be blocked by ESC14 IgG and vice versa, whereas F19 (28) did not compete with either of the ESC antibodies for FAP binding (Supplementary Fig. S3). These results suggest that antibodies ESC11 and ESC14 recognize the same epitope or overlapping/spatially close epitopes that are different from the epitope recognized by the F19 antibody.

Table 1. Apparent affinities of anti-FAP antibodies on huFAP and muFAP.

	K_DApp on huFAP [nmol/L]	K_DApp on muFAP [nmol/L]
ESC11 Fab fragment	4.7 ± 1.6	51 ± 11
ESC14 Fab fragment	205 ± 35	251 ± 42
ESC11 IgG1	1.1 ± 0.1	1.8 ± 0.3
ESC14 IgG1	1.1 ± 0.4	2.1± 0.5
vF19 IgG1	4.2 ± 0.6	n.d.[a]

[a]n.d., not defined.

ESC11 and ESC14 IgG1 induce downmodulation and internalization of surface FAP

Incubation of SK-MEL-187, a FAP-expressing melanoma cell line, with F19, ESC11, or ESC14 on ice resulted in detectable surface staining. However, incubation at 37°C for 3 hours with ESC11 or ESC14, but not with F19, induced internalization of FAP-antibody complexes (Fig. 2A and B). This was not observed with monovalent Fabs indicating that cross-linking of FAP molecules by bivalent IgG1 was essential (data not shown). Internalization of surface FAP occurred very rapidly. Already after 20 minutes at 37°C, an almost complete colocalization of internalized antibody with early endosomes could be observed, whereas after 40 minutes, colocalization with LAMP-1, a marker for late endosomes and lysosomes (Fig. 2C) was seen. We next tested pharmacologic inhibitors of both dynamin-dependent endocytosis (dynasore) and macropinocytosis (EIPA)

Downloaded from http://aacrjournals.org/clincancerres/article-pdf/18/22/6208/2007966/6208.pdf by guest on 17 February 2026

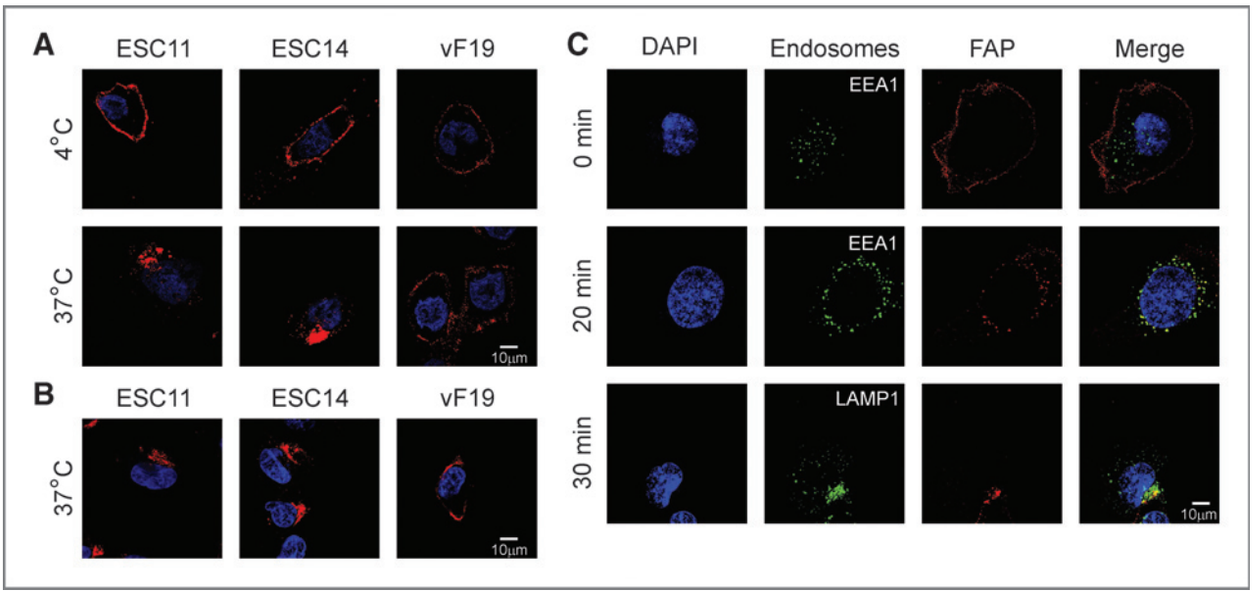


Figure 2. Antibody-induced internalization of FAP. A, representative confocal microscopy images of SK-Mel-187 cells incubated with anti-FAP antibodies for 3 hours. FAP staining is shown in red. B, spatial localization of DyLight 549-labeled anti-FAP antibodies on SK-MEL-187 cells after 3 hours incubation at 37°C. C, colocalization of FAP and endosomes: SK-Mel-187 cells were incubated with ESC11 IgG1 and localization of FAP (DyLight 549-F19; red) was followed by staining early endosomes (EEA1; green) and late endosomes/early lysosomes (LAMP-1; green). The merge of the 3 images is shown on the right. Yellow indicates colocalization of FAP with endosomal markers.

to investigate the mechanism of endocytosis. Dynasore inhibited antibody-mediated FAP internalization (Supplementary Fig. S4A), whereas EIPA had no effect (Supplementary Fig. S4B), showing that endocytosis is mediated by a dynamin-dependent mechanism.

After overnight incubation with ESC11 and ESC14 antibodies, only very little FAP was detectable by flow cytometry on the surface of SK-MEL-187 cells. In contrast, still around 80% of cell-surface FAP could be detected after prolonged incubation with vF19 (Fig. 3A). We next investigated the time and concentration dependency of the observed FAP downmodulation for ESC11. Overnight internalization was concentration dependent and the half-maximal effective concentration (EC_{50}) was 3.3 ± 0.5 nmol/L (Fig. 3B). At this concentration, most of the FAP epitopes are occupied by ESC11 antibody, which presumably results in rafting of FAP molecules and concomitant internalization. To assess time dependency, we then chose a concentration of 200 nmol/L at which FAP downmodulation is expected to be more than 90%. FAP was rapidly internalized, and the majority of FAP molecules disappeared from the cell surface within 1 hour (Fig. 3C). When excess antibody was removed after overnight incubation, full FAP expression was restored not before 3 days after antibody removal (Fig. 3D). In contrast, FAP expression remained low when ESC11 was present over the entire observation period.

mAb ESC11 specifically accumulates in human melanoma xenografts *in vivo*

ESC11, ESC14, vF19, and A33 were conjugated with CHX-A″-DTPA and subsequently labeled with ^{177}Lu. Radiochemical purity was more than 95% by FPLC for all 4 antibodies, and the specific activities were 0.4 to 0.45 MBq/μg. Immunoreactivity of the radiolabeled antibodies was between 50% and 70% as determined by Lindmo analysis. All 3 ^{177}Lu-labeled FAP-binding antibodies bound specifically to SK-MEL-187 cells and could be displaced with increasing amounts of unlabeled antibody, whereas only a low amount of nonspecific binding could be observed on the FAP-negative SK-MEL-16 cells (data not shown). Accordingly, SPECT/CT imaging 72 hours after injection showed high and specific uptake of ^{177}Lu-ESC11 in the SK-MEL-187 tumor (Fig. 4A), but low uptake in a SK-MEL-16 xenograft. Specific uptake was also observed with ^{177}Lu-vF19 in the FAP-expressing tumor (Fig. 4B), whereas the control antibody ^{177}Lu-A33 did not accumulate in either tumor (Fig. 4C).

Biodistribution data showed very high uptake of the 3 antibodies in FAP-expressing tumors 72 hours after injection and low activity in nontargeted organs (Fig. 4D). Notably, ^{177}Lu-vF19 and, to a lesser extent, ^{177}Lu-ESC14 showed higher accumulation in the spleen than ^{177}Lu-ESC11, and cleared faster from the blood, which resulted in a reduced uptake in the tumors.

The *in vivo* biodistribution of ^{177}Lu- ESC11 was further studied over time in nude mice bearing human SK-MEL-187 tumor xenografts. We found a high (36% of the injected dose per gram of tumor tissue after 48 hours) and prolonged uptake of ^{177}Lu- ESC11, whereas its presence in blood and other organs was relatively low (Fig. 4E). Radioactivity in melanoma xenografts accumulated until approximately 48 hours after injection. After this time point, uptake values in the tumors remained high,

Downloaded from http://aacrjournals.org/clincancerres/article-pdf/18/22/6208/2007966/6208.pdf by guest on 17 February 2026

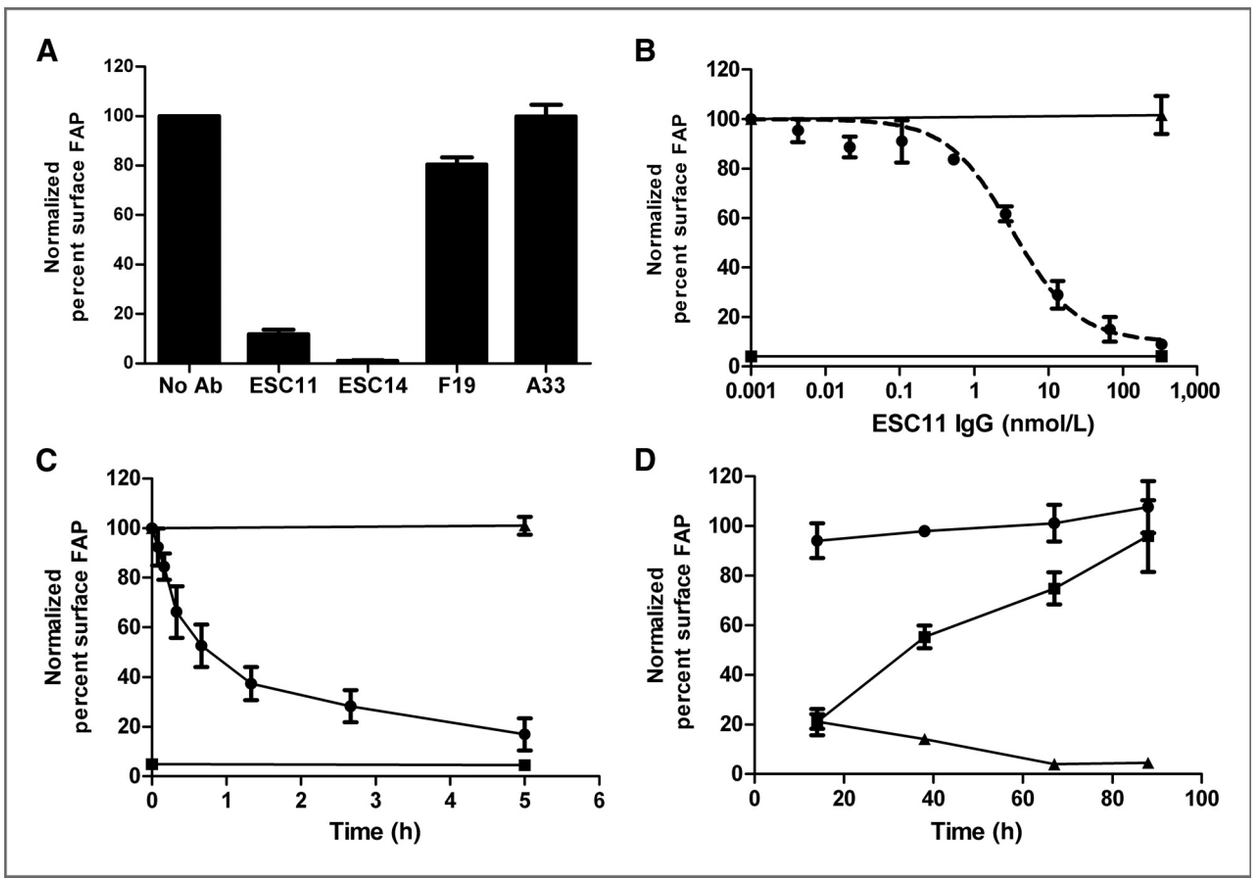


Figure 3. Comparative FAP downmodulation capabilities of anti-FAP antibodies *in vitro*: A, SK-Mel-187 cells were incubated overnight with the indicated antibodies. B, FAP downmodulation pattern after incubation with ESC11 IgG1 on FAP-positive [SK-Mel-187; solid circles with fitted sigmoid dose–response curve (dashed line)] and FAP-negative (SK-Mel-16; solid squares) human melanoma cell lines and with isotype control antibody, A33 (on SK-Mel-187; solid triangles). C, time-dependent FAP downmodulation by ESC11 IgG1 on SK-Mel-187 cells (solid circles) and SK-Mel-16 cells (solid squares) and isotype control antibody (solid triangles) on SK-Mel-187 cells at $t = 0$ (initial) and $t = 5$ (final) time points. D, time kinetics of FAP reappearance on SK-Mel-187 cell surface. Solid squares, ESC11 added at $t = 0$ and removed at $t = 14$ hours; solid triangles, ESC11 added at $t = 0$; solid circles, no antibody added. All results are presented as percent values normalized to receptor-positive cells in the absence of any antibody. Error bars, SD ($n = 3$).

but also became more variable in the individual mice, most likely due to the inhomogeneous tumor growth observed for this tumor model.

Radioimmunotherapy of established melanoma xenografts with ^{177}Lu-labeled FAP-specific antibodies

Next, we investigated the therapeutic efficacy of a single dose of the ^{177}Lu radioimmunoconjugates *in vivo*. We estimated a dose of 8 MBq to be therapeutically active (31) and this dose has been shown to be well below the maximum tolerated dose in this mouse strain with other antibodies displaying similar biodistribution properties. Eight MBq (15 μg) ^{177}Lu-labeled antibodies were injected intravenously into nude mice bearing established subcutaneous human melanoma tumors (~150 mm^3) 5 days after tumor implantation. Tumor growth was delayed with all 3 anti-FAP antibodies and ^{177}Lu-ESC11 exhibited the most pronounced growth delay (Fig. 5A). Analysis of survival curves (Fig. 5B) showed an increase of median survival from 18 days (^{177}Lu-A33) to 32 days (^{177}Lu-vF19), 43 days (^{177}Lu-ESC14), and more than 43 days (^{177}Lu-ESC11) after tumor implantation. Additional mice were sacrificed on day 0, 3, and 7 after injection of radioimmunoconjugates, and tumor specimens were processed for immunohistochemistry. We found a substantial reduction of proliferating (Ki-67$^+$) tumor cells in samples taken after 3 and 7 days after injection of ^{177}Lu- ESC11 but not of the control conjugate (Fig. 5C). In addition, we observed increasing cell-free areas over time in the tumors treated with radiolabeled ESC11 (Fig. 5D).

Discussion

We here describe the selection of novel human–mouse FAP-specific antibodies which downmodulate FAP expression from the surface of tumor cells, thus converting them into FAP-negative cells. Therapeutic strategies that aim at the complete downmodulation of FAP expression from the cellular surface might be promising approaches *per se*, as FAP is involved in cell invasion and metastatic processes of many cancers. Thus, antibody-induced internalization of

Downloaded from http://aacrjournals.org/clincancerres/article-pdf/18/22/6208/2007966/6208.pdf by guest on 17 February 2026

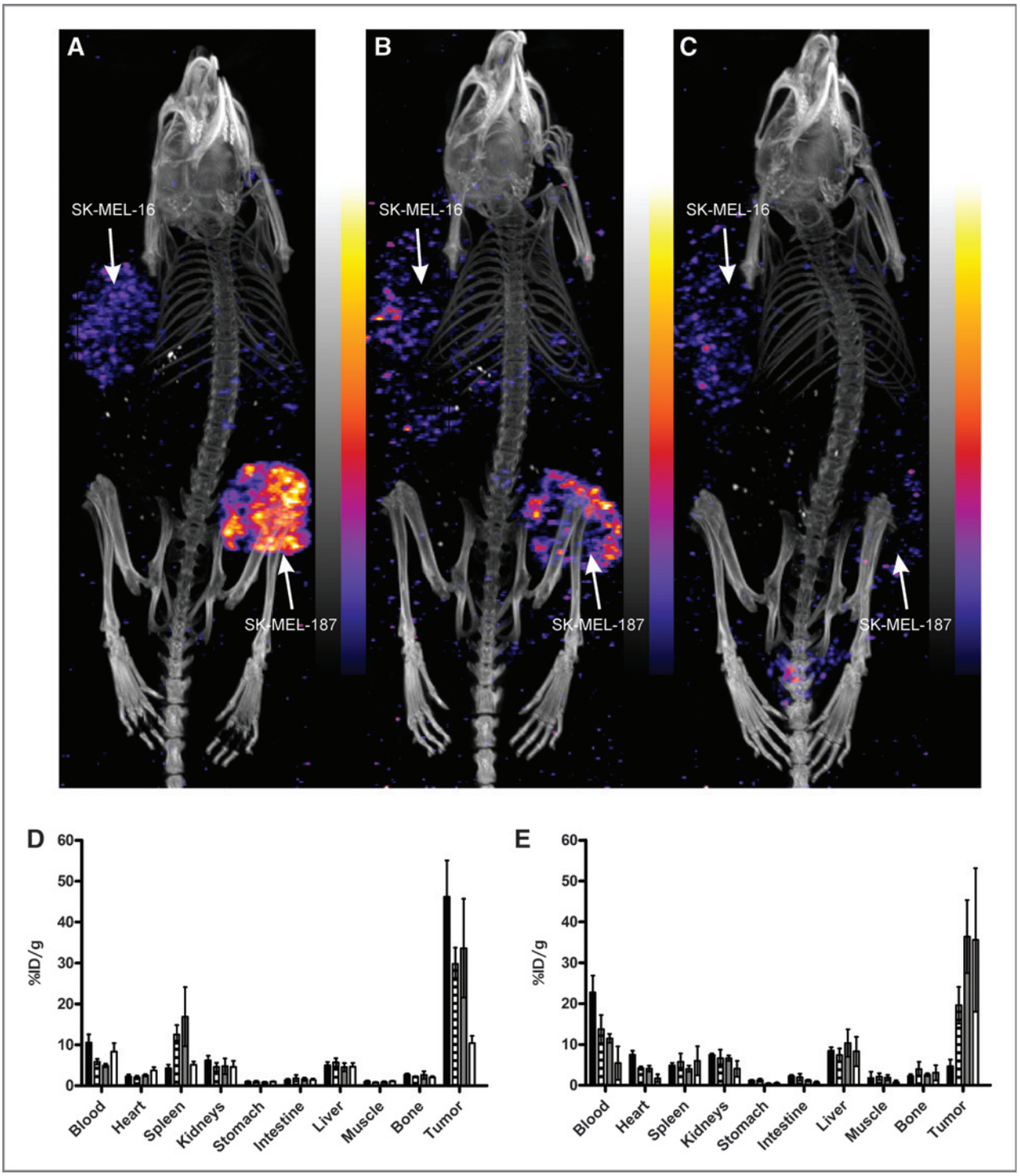


Figure 4. Biodistribution of 177Lu-labeled FAP-specific antibodies. Post mortem SPECT/CT images showing biodistribution of (A) ^{177}Lu-CHX-A″-DTPA-ESC11, (B) ^{177}Lu-CHX-A″-DTPA-vF19, and (C) ^{177}Lu-CHX-A″-DTPA-A33 in nude mice 72 hours after injection. D, biodistribution of ^{177}Lu-labeled antibodies in mice bearing SK-Mel-187 xenografts 72 hours after injection. ^{177}Lu-ESC11 (black bars), ^{177}Lu-ESC14 (striped bars), ^{177}Lu-vF19 (grey bars), and ^{177}Lu-A33 (white bars). E, time-dependent biodistribution of ^{177}Lu-ESC11 in mice bearing SK-Mel-187 xenografts after 3 hours (black bars), 24 hours (striped bars), 48 hours (grey bars), and 7 days (white bars). Results are presented as percentage of injected dose per gram of tissue. Error bars represent SD ($n = 4$; D).

Downloaded from http://aacrjournals.org/clincancerres/article-pdf/18/22/6208/2007966/6208.pdf by guest on 17 February 2026

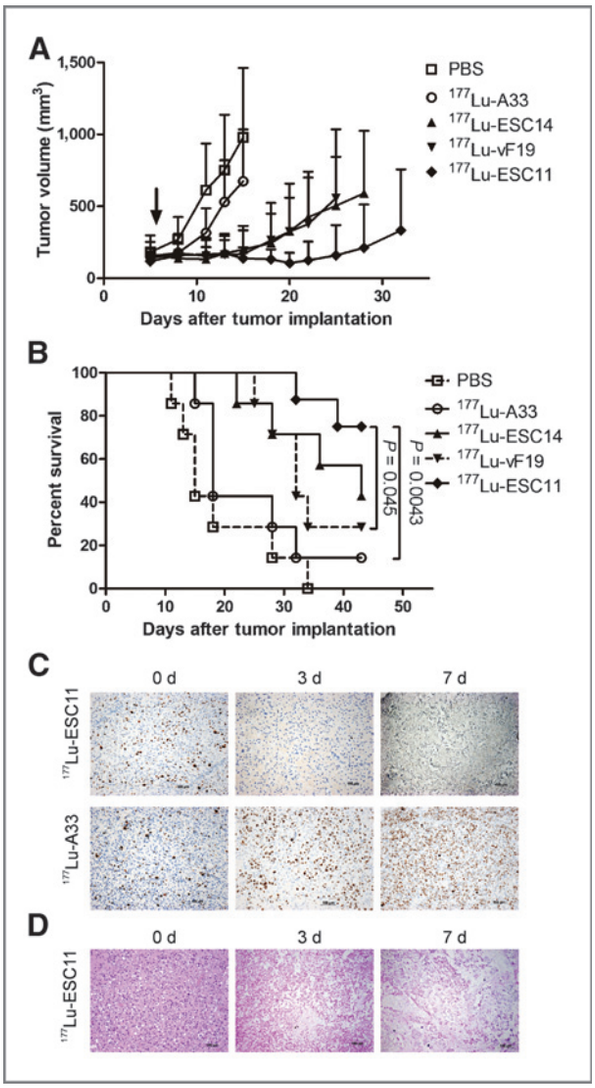


Figure 5. Radioimmunotherapy in nude mice bearing subcutaneous FAP-positive SK-MEL-187 tumors: Tumor bearing mice were treated intravenously with 8 MBq (15 μg) ^{177}Lu-labeled antibodies or PBS 5 days after tumor implantation (arrow). A, tumor growth curves showing mean tumor volumes + SD. Curves were plotted until the first tumor per group reached 1,000 m^3. B, Kaplan–Meier survival curves of treated and control groups. *P* values were obtained with a log-rank test. Ki-67 stained (C) and H&E stained–tumor slices (D) on days 0, 3, and 7 after injection of radiolabeled antibodies. Scale bar, 100 μm.

cell surface–expressed FAP could provide major therapeutic impact by disturbing the various interactions on the cellular membrane, for example, the formation of functional invadopodia.

But more importantly, the rapid internalization renders them perfect carrier proteins for the targeted destruction of FAP positive carcinoma-associated fibroblasts or tumor cells. These approaches have the potential to be much more efficient than therapy with naked antibodies (32). While internalization of the antibody is not a prerequisite for successful radioimmunotherapy with a β-particle emitting radionuclide like ^{177}Lu, it becomes a clear advantage when using α-particle or Auger-electron emitting radionuclides instead. In these cases, the vicinity of the internalized radionuclide to the cellular nucleus augments the therapeutic efficacy by introducing more damage to the radiation-sensitive DNA. Antibody–drug conjugates are a second example for which internalization is an important feature, especially when the drug is coupled to the antibody by an acid-labile linker releasing the cytotoxic drug in the acidic lysosomes.

We have chosen human melanoma as a model system because the interaction between tumor cells and carcinoma-associated fibroblasts seems to be crucial for tumor growth and the development of drugs resistance (33). As shown by Flach and colleagues, melanoma cells stimulate the recruitment of fibroblasts and activate them by a so far unknown mechanism. In turn, these activated fibroblasts contribute to melanoma progression by providing both structural and chemical support (33). Incomplete abolishment of tumor cells by a short duration of kinase inhibitor therapy led to a transient reduction of tumor cells that was counteracted by an accelerated regrowth of tumor cells supported by the large fibroblast population that remained posttreatment. According to their model, the sole elimination of tumor cells is insufficient to provide tumor control and only a combined approach targeting tumor cells and carcinoma-associated fibroblasts simultaneously will lead to long lasting remissions.

FAP is not ubiquitously expressed in human melanoma at all stages of disease but is transiently present during the development of malignancy, and is routinely confined to the stromal fibroblasts in metastatic melanoma (34). However, high expression levels of FAP have been shown to correlate with a pronounced invasive phenotype *in vitro* (35) and have recently been postulated to contribute to transmigration of melanoma cells through the blood-brain barrier (36).

In this study, we compared the *in vivo* targeting properties of the human–mouse cross-reactive antibodies ESC11 and ESC14 to vF19. In a model with relatively high antigen expression on the tumor cells, high accumulation of up to 50% of the injected dose per gram tumor was observed. The only previously reported biodistribution experiment with a FAP-targeting antibody in mice was a study with human skin-grafted SCID mice bearing breast cancer tumors and a ^{131}I-labeled antibody (37). There, much lower accumulation in the tumor and less favorable tumor-to-organ ratios were achieved, presumably as a result of the tumor model and the choice of the metabolically less stable radiolabel. In phase I clinical trials, ^{131}I-labeled mAb F19 and its CDR-grafted humanized variant have been used to study pharmacokinetics, biodistribution, and imaging characteristics in patients with metastatic cancer (25, 38, 39). FAP was efficiently targeted by mAb F19 in all patients and its expression was confined to the stroma of metastatic lesions. Given the high expression of FAP in human cancers and the

Downloaded from http://aacrjournals.org/clincancerres/article-pdf/18/22/6208/2007966/6208.pdf by guest on 17 February 2026

restriction to diseased tissue, FAP is a promising target both for imaging and radioimmunotherapy.

In particular, targeting stromal fibroblasts instead of tumor cells has several appealing advantages: the highly vascularized stroma is thought to be reached more efficiently by bulky molecules such as monoclonal antibodies. Antigen expression is considered to be more stable in carcinoma-associated fibroblasts than in highly proliferating cancer cells.

Furthermore, in many human epithelial cancers, stromal fibroblasts are highly abundant, and the cross-fire effect of low energy β-emitting radionuclides (penetration of 2 mm in tissue) additionally contributes to the eradication of antigen-negative tumor cells and to a homogenous deposition of the dose within the tumor tissue. A recent study showed that antitumor immunity is suppressed by FAP-positive stromal cells (21), which adds to the importance of FAP in tumor physiology. Thus, human–mouse cross-reactive FAP-specific antibodies are excellent tools to address this phenomenon *in vivo* by specific targeting of FAP-positive stromal fibroblasts and may help to unravel the mechanisms involved in local immunosuppression and tumor promotion.

In conclusion, we have developed novel fully human antibodies with excellent *in vivo* targeting properties. Because of their efficient internalization and targeting to the lysosomes, they are promising scaffolds for future development of antibody–drug conjugates or radioimmunotherapeutics.

Disclosure of Potential Conflicts of Interest

No potential conflicts of interest were disclosed.

Authors' Contributions

Conception and design: E. Fischer, T. Wuest, A.M. Scott, M. van den Broek, S. Bauer, C. Renner

Development of methodology: E. Fischer, K. Chaitanya, T. Wuest, A. Wadle, A.M. Scott, M. van den Broek, S. Bauer, C. Renner

Acquisition of data (provided animals, acquired and managed patients, provided facilities, etc.): E. Fischer, K. Chaitanya, T. Wuest, S. Bauer

Analysis and interpretation of data (e.g., statistical analysis, biostatistics, computational analysis): E. Fischer, K. Chaitanya, T. Wuest, A. Wadle, S. Bauer, C. Renner

Writing, review, and/or revision of the manuscript: E. Fischer, K. Chaitanya, T. Wuest, A.M. Scott, M. van den Broek, S. Bauer, C. Renner

Administrative, technical, or material support (i.e., reporting or organizing data, constructing databases): T. Wuest, R. Schibli, S. Bauer, C. Renner

Study supervision: E. Fischer, M. van den Broek, R. Schibli, S. Bauer, C. Renner

Acknowledgments

The authors thank Susan Cohrs and Sascha Kleber for excellent technical assistance.

Grant Support

This study was supported by Ludwig Institute for Cancer Research/Atlantic Philanthropies (to C. Renner), Zürcher Krebsliga (to T. Wuest and C. Renner), Krebsforschung Schweiz (to T. Wuest, E. Fischer, and C. Renner), and the University of Zürich (Forschungskredit to E. Fischer and S. Bauer).

The costs of publication of this article were defrayed in part by the payment of page charges. This article must therefore be hereby marked *advertisement* in accordance with 18 U.S.C. Section 1734 solely to indicate this fact.

Received February 23, 2012; revised August 28, 2012; accepted August 31, 2012; published OnlineFirst September 19, 2012.

References

1. Bhowmick NA, Neilson EG, Moses HL. Stromal fibroblasts in cancer initiation and progression. Nature 2004;432:332–7.
2. Hwang RF, Moore T, Arumugam T, Ramachandran V, Amos KD, Rivera A, et al. Cancer-associated stromal fibroblasts promote pancreatic tumor progression. Cancer Res 2008;68:918–26.
3. Karnoub AE, Dash AB, Vo AP, Sullivan A, Brooks MW, Bell GW, et al. Mesenchymal stem cells within tumour stroma promote breast cancer metastasis. Nature 2007;449:557–63.
4. Dohi O, Ohtani H, Hatori M, Sato E, Hosaka M, Nagura H, et al. Histogenesis-specific expression of fibroblast activation protein and dipeptidylpeptidase-IV in human bone and soft tissue tumours. Histopathology 2009;55:432–40.
5. Huber MA, Kraut N, Park JE, Schubert RD, Rettig WJ, Peter RU, et al. Fibroblast activation protein: differential expression and serine protease activity in reactive stromal fibroblasts of melanocytic skin tumors. J Invest Dermatol 2003;120:182–8.
6. Aoyama A, Chen WT. A 170-kDa membrane-bound protease is associated with the expression of invasiveness by human malignant melanoma cells. Proc Natl Acad Sci U S A 1990;87:8296–300.
7. Kelly T. Evaluation of seprase activity. Clin Exp Metastasis 1999;17:57–62.
8. Garin-Chesa P, Old LJ, Rettig WJ. Cell surface glycoprotein of reactive stromal fibroblasts as a potential antibody target in human epithelial cancers. Proc Natl Acad Sci U S A 1990;87:7235–9.
9. Aggarwal S, Brennen WN, Kole TP, Schneider E, Topaloglu O, Yates M, et al. Fibroblast activation protein peptide substrates identified from human collagen I derived gelatin cleavage sites. Biochemistry (Mosc) 2008;47:1076–86.
10. Park JE, Lenter MC, Zimmermann RN, Garin-Chesa P, Old LJ, Rettig WJ. Fibroblast activation protein, a dual specificity serine protease expressed in reactive human tumor stromal fibroblasts. J Biol Chem 1999;274:36505–12.
11. Christiansen VJ, Jackson KW, Lee KN, McKee PA. Effect of fibroblast activation protein and alpha2-antiplasmin cleaving enzyme on collagen types I, III, and IV. Arch Biochem Biophys 2007;457:177–86.
12. Cheng JD, Valianou M, Canutescu AA, Jaffe EK, Lee HO, Wang H, et al. Abrogation of fibroblast activation protein enzymatic activity attenuates tumor growth. Mol Cancer Ther 2005;4:351–60.
13. Ghersi G, Dong H, Goldstein LA, Yeh Y, Hakkinen L, Larjava HS, et al. Regulation of fibroblast migration on collagenous matrix by a cell surface peptidase complex. J Biol Chem 2002;277:29231–41.
14. Wang XM, Yu DM, McCaughan GW, Gorrell MD. Fibroblast activation protein increases apoptosis, cell adhesion, and migration by the LX-2 human stellate cell line. Hepatology 2005;42:935–45.
15. Kennedy A, Dong H, Chen D, Chen WT. Elevation of seprase expression and promotion of an invasive phenotype by collagenous matrices in ovarian tumor cells. Int J Cancer 2009;124:27–35.
16. Mueller SC, Ghersi G, Akiyama SK, Sang QX, Howard L, Pineiro-Sanchez M, et al. A novel protease-docking function of integrin at invadopodia. J Biol Chem 1999;274:24947–52.
17. Wolf BB, Quan C, Tran T, Wiesmann C, Sutherlin D. On the edge of validation–cancer protease fibroblast activation protein. Mini Rev Med Chem 2008;8:719–27.
18. Lee HO, Mullins SR, Franco-Barraza J, Valianou M, Cukierman E, Cheng JD. FAP-overexpressing fibroblasts produce an extracellular matrix that enhances invasive velocity and directionality of pancreatic cancer cells. BMC Cancer 2011;11:245.
19. Niedermeyer J, Enenkel B, Park JE, Lenter M, Rettig WJ, Damm K, et al. Mouse fibroblast-activation protein–conserved Fap gene organization and biochemical function as a serine protease. Eur J Biochem 1998;254:650–4.

Downloaded from http://aacrjournals.org/clincancerres/article-pdf/18/22/6208/2007966/6208.pdf by guest on 17 February 2026

20. Huang Y, Simms AE, Mazur A, Wang S, Leon NR, Jones B, et al. Fibroblast activation protein-alpha promotes tumor growth and invasion of breast cancer cells through non-enzymatic functions. Clin Exp Metastasis 2011;28:567–79.
21. Kraman M, Bambrough PJ, Arnold JN, Roberts EW, Magiera L, Jones JO, et al. Suppression of antitumor immunity by stromal cells expressing fibroblast activation protein-alpha. Science 2010;330:827–30.
22. Cohen SJ, Alpaugh RK, Palazzo I, Meropol NJ, Rogatko A, Xu Z, et al. Fibroblast activation protein and its relationship to clinical outcome in pancreatic adenocarcinoma. Pancreas 2008;37:154–8.
23. Henry LR, Lee HO, Lee JS, Klein-Szanto A, Watts P, Ross EA, et al. Clinical implications of fibroblast activation protein in patients with colon cancer. Clin Cancer Res 2007;13:1736–41.
24. Hofheinz RD, al-Batran SE, Hartmann F, Hartung G, Jager D, Renner C, et al. Stromal antigen targeting by a humanised monoclonal antibody: an early phase II trial of sibrotuzumab in patients with metastatic colorectal cancer. Onkologie 2003;26:44–8.
25. Scott AM, Wiseman G, Welt S, Adjei A, Lee FT, Hopkins W, et al. A Phase I dose-escalation study of sibrotuzumab in patients with advanced or metastatic fibroblast activation protein-positive cancer. Clin Cancer Res 2003;9:1639–47.
26. Ostermann E, Garin-Chesa P, Heider KH, Kalat M, Lamche H, Puri C, et al. Effective immunoconjugate therapy in cancer models targeting a serine protease of tumor fibroblasts. Clin Cancer Res 2008;14:4584–92.
27. Bauer S, Adrian N, Williamson B, Panousis C, Fadle N, Smerd J, et al. Targeted bioactivity of membrane-anchored TNF by an antibody-derived TNF fusion protein. J Immunol 2004;172:3930–9.
28. Bauer S, Adrian N, Fischer E, Kleber S, Stenner F, Wadle A, et al. Structure-activity profiles of Ab-derived TNF fusion proteins. J Immunol 2006;177:2423–30.
29. de Haard HJ, van Neer N, Reurs A, Hufton SE, Roovers RC, Henderikx P, et al. A large non-immunized human Fab fragment phage library that permits rapid isolation and kinetic analysis of high affinity antibodies. J Biol Chem 1999;274:18218–30.
30. Knogler K, Grünberg J, Novak-Hofer I, Zimmermann K, Schubiger PA. Evaluation of 177Lu-DOTA-labeled aglycosylated monoclonal anti-L1-CAM antibody chCE7: influence of the number of chelators on the *in vitro* and *in vivo* properties. Nucl Med Biol 2006;33:883–9.
31. Fischer E, Grunberg J, Cohrs S, Hohn A, Waldner-Knogler K, Jeger S, et al. L1-CAM-targeted antibody therapy and (177) Lu-Radioimmunotherapy of disseminated ovarian cancer. Int J Cancer 2011;130:2715–21.
32. Casi G, Neri D. Antibody-drug conjugates: basic concepts, examples and future perspectives. J Control Release 2012;161:422–8.
33. Flach EH, Rebecca VW, Herlyn M, Smalley KS, Anderson AR. Fibroblasts contribute to melanoma tumor growth and drug resistance. Mol Pharm 2011;8:2039–49.
34. Rettig WJ, Garin-Chesa P, Healey JH, Su SL, Ozer HL, Schwab M, et al. Regulation and heteromeric structure of the fibroblast activation protein in normal and transformed cells of mesenchymal and neuroectodermal origin. Cancer Res 1993;53:3327–35.
35. Monsky WL, Lin CY, Aoyama A, Kelly T, Akiyama SK, Mueller SC, et al. A potential marker protease of invasiveness, seprase, is localized on invadopodia of human malignant melanoma cells. Cancer Res 1994;54:5702–10.
36. Fazakas C, Wilhelm I, Nagyoszi P, Farkas AE, Hasko J, Molnar J, et al. Transmigration of melanoma cells through the blood-brain barrier: role of endothelial tight junctions and melanoma-released serine proteases. PloS ONE 2011;6:e20758.
37. Tahtis K, Lee FT, Wheatley JM, Garin-Chesa P, Park JE, Smyth FE, et al. Expression and targeting of human fibroblast activation protein in a human skin/severe combined immunodeficient mouse breast cancer xenograft model. Mol Cancer Ther 2003;2:729–37.
38. Welt S, Divgi CR, Scott AM, Garin-Chesa P, Finn RD, Graham M, et al. Antibody targeting in metastatic colon cancer: a phase I study of monoclonal antibody F19 against a cell-surface protein of reactive tumor stromal fibroblasts. J Clin Oncol 1994;12:1193–203.
39. Tanswell P, Garin-Chesa P, Rettig WJ, Welt S, Divgi CR, Casper ES, et al. Population pharmacokinetics of antifibroblast activation protein monoclonal antibody F19 in cancer patients. Br J Clin Pharmacol 2001;51:177–80.

Downloaded from http://aacrjournals.org/clincancerres/article-pdf/18/22/6208/2007966/6208.pdf by guest on 17 February 2026

SUPPLEMETARY DATA

Antibody selection by phage display. 10^{13} Phages were blocked in 2% milk powder in PBS and pre-absorbed three times with 50 µl anti-huFAP IgG-coated protein A beads preparations which beforehand were incubated with lysates from HT1080 cells. In this pre-absorption step, the library was depleted from phages that bind to either protein A, bound IgG, or any coprecipitated protein from the HT1080 lysates. Pre-absorbed phages were then incubated with immunocaptured huFAP for 1 h at room temperature, washed six times with PBS 0.1% Tween20, two times with PBS, and subsequently eluted with 100 mM triethylamine. Neutralized phages were amplified in *Escherichia coli* TG-1 using M13K07 helper phage. Four rounds of selection with decreasing antigen concentration were performed (50, 25, 12.5, and 6.5 µl of immunocaptured FAP suspension). Prior to selection rounds four and five, an additional depletion step on 50 µl immunocaptured CD26 suspension was included to remove FAP-binders that cross-react with CD26. To enrich the phage pool for binders that recognize muFAP, a fifth round was appended by incubating the phages with HEK293 muFAP expressing cells.

SUPPLEMENTARY FIGURE LEGENDS

Figure S1. Immunoprecipitation of huFAP from HT1080 FAP$^+$ cells using anti-huFAP antibody. 5x10^7 HT1080 FAP$^+$ or HT1080 cells were solubilized in 5 ml lysis buffer (50 mM Tris-HCl, 150 mM NaCl, pH 7.4, 0.7% w/v β-octylglucopyranoside) by vortexing for 15 min at 4°C. Cell debris was removed by centrifugation and the supernatant was incubated for 4 hrs at 4°C with 50 µl anti-huFAP antibody coated protein A Dynabead suspension (Invitrogen). Beads were removed from suspension using a magnetic rack, washed five times with PBS 0.1% Tween 20 (PBST), and stored at -80°C in 100 µl PBS. Accordingly, recombinant CD26 was immunoprecipitated with an anti-CD26 mAb (Santa Cruz Biotechnology, Santa Cruz, CA). Purity and functionality of the immunoprecipitates were analyzed by SDS-PAGE, western blot and DPP activity assay.

A. Coomassie blue stained SDS-PAGE gel and **B.** Corresponding western blot probed with F19 antibody. **C.** Dipeptidyl-peptidase activity in immunocaptured FAP from HT1080 FAP$^+$ and the parental HT1080 lysates. A.U., arbitrary units. HC, heavy chain of F19 antibody.

Figure S2. Recombinant expression of Fab fragments and antibodies. Coomassie-staining of acrylamide-gel after SDS-PAGE of ESC11 and ESC14 IgG and Fab fragments under reducing and non-reducing conditions.

Figure S3. Epitope mapping by competitive binding to HT1080 huFAP^{+}. For measuring the competitive binding of ESC11 and ESC14, Fab fragments were titered on HT1080 FAP^{+} cells and binding was determined by flow cytometry. The concentration resulting in 90% of the maximal binding was used for the competition assay. HT1080 FAP^{+} were incubated with the indicated antibodies at 5 µg/ml for 20 min at 4°C, then the ESC11/ESC14 Fab fragments or PBS added at the pre-determined concentrations and incubated for 20 min at 4°C. Cells were washed once with PBS at 4°C and fixed with 2% PFA on ice. Bound Fab fragment was detected and analyzed by flow cytometry as described.
A. Competitive inhibition of ESC11 Fab and **B** of ESC14 Fab binding by preincubation with the indicated antibodies at 5 µg/ml. One representative experiment of three is shown with mean and s.d. of triplicates.

Figure S4. **Inhibition of FAP internalization mediated by ESC11 IgG1 *in vitro*:**

A. Effect of dynasore on FAP internalization: Representative pictures for 0 µM (a and b), 50 µM (c and d) and 100 µM (e and f) dynasore concentrations, in presence of ESC11 IgG1 were obtained. Top panel (a, c and e) shows the samples maintained at 0°C and bottom panel (b, d and f) at 37°C. FAP staining is shown in red. **B.** Effect of EIPA on FAP internalization: Representative pictures for 0 µM (a and b) and 10 µM (c and d) EIPA concentrations, in presence of ESC11 IgG1 were obtained. Top panel (a and c) shows the samples maintained at 0°C and bottom panel (b and d) at 37°C. FAP staining is shown in red. Scale bar represents 10 micrometers. All images were acquired in SP5 CLSM and processed using ImageJ software.

Table S1: Selection strategy

Selection Round	Preabsorption step	Selection	Output*
1	50 µl mock immunocapture	50µl immunocaptured FAP	
2	50 µl mock immunocapture	25µl immunocaptured FAP	
3	50 µl mock immunocapture	10µl immunocaptured FAP	0/0/90
4	50 µl mock immunocapture 50 µl immunocaptured CD26	5µl immunocaptured FAP	4/1/90
5	50 µl immunocaptured CD26 10^7 HEK293 cells	10^6 HEK293 muFAP cells	13/8/90

* huFAP specific phages/huFAP-muFAP crossreactive Phages/total screened phages